Selective Growth of Gold onto Copper Indium Sulfide Selenide Nanoparticles

Elena Witt, Jürgen Parisi, and Joanna Kolny-Olesiak

University of Oldenburg, Institute of Physics, Energy and Semiconductor Research, Carl-von-Ossietzky-Straße 9–11, 26129 Oldenburg

Reprint requests to J. K.-O.; E-mail: joanna.kolny@uni-oldenburg.de

Z. Naturforsch. **68a,** 398 – 404 (2013) / DOI: 10.5560/ZNA.2013-0016
Received January 23, 2013 / published online April 10, 2013

Hybrid nanostructures are interesting materials for numerous applications in chemistry, physics, and biology, due to their novel properties and multiple functionalities. Here, we present a synthesis of metal–semiconductor hybrid nanostructures composed of nontoxic I-III-VI semiconductor nanoparticles and gold. Copper indium sulfide selenide (CuInSSe) nanocrystals with zinc blende structure and trigonal pyramidal shape, capped with dodecanethiol, serve as an original semiconductor part of a new hybrid nanostructure. Metallic gold nanocrystals selectively grow onto vertexes of these CuInSSe pyramids. The hybrid nanostructures were studied by transmission electron microscopy, energy dispersive X-ray analysis, X-ray diffraction, and UV-Vis-absorption spectroscopy, which allowed us conclusions about their growth mechanism. Hybrid nanocrystals are generated by replacement of a sacrificial domain in the CuInSSe part. At the same time, small selenium nanocrystals form that stay attached to the remaining CuInSSe/Au particles. Additionally, we compare the synthesis and properties of CuInSSe-based hybrid nanostructures with those of copper indium disulfide ($CuInS_2$). $CuInS_2$/Au nanostructures grow by a different mechanism (surface growth) and do not show any selectivity.

Key words: Copper Indium Selenide; Copper Indium Sulfide; Metal–Semiconductor Hybrid; Nanostructures; Gold; Heterogeneous Nucleation.

1. Introduction

Hybrid nanostructures are of high interest in academic research. The presence of different materials in one system opens up many possibilities to change properties from these of each single component or of their physical blend [1 – 6]. Due to such unique opportunity, hybrid nanomaterials find wide applications in physical, chemical, and biological research [1, 7 – 11].

Metal–semiconductor hybrid nanostructures are one important class of these multifunctional materials. A direct contact between a metal nanocrystal and a semiconductor nanoparticle facilitates charge separation after exciton generation in the semiconductor [12, 13], which might be useful for solar energy conversion [14] and heterogeneous catalysis [15]. The metal part can be used to apply an electrical contact to the hybrid structure and to increase the electrical conductance of nanomaterials, which is important for opto-electronic devices [16]. Directly connecting metal and semiconductor nanoparticles together gives an opportunity to influence the optical properties of both materials. The plasmon resonance of metal nanocrystals can be shifted [1], as well as the photoluminescence intensity of semiconductor nanoparticles can be changed [1, 17], the latter could be interesting for applications in biological detection. Furthermore, self-assembly methods already well developed for metal nanocrystals can be applied to form superstructures of semiconductor–metal hybrid materials [17]. Thus, hybrid nanostructures possess characteristics making them suitable for building blocks for the development of nanomaterial-based devices.

The synthesis route of the growth of gold nanocrystals onto semiconductor nanoparticles was reported by Mokari et al. [17]. CdSe nanorods and tetrapods react with gold stock solution yielding CdSe/Au hybrid nanostructures. This simple synthetic method can be applied for many systems, such as CdS [16, 18], CdTe [1], PbS [14, 19, 20], PbSe [20] nanomaterials.

To avoid the toxicity of cadmium und lead chalcogenides, the research tends to alternative semiconductor materials, in particular, to ternary I-III-VI semiconductor nanocrystals [21 – 24]. However, to the best of our knowledge, there are just a few reports on the formation of metal-I-III-VI-semiconductor hybrid materials [25, 26]. In the following, we present our experiments on the growth of gold nanocrystals (Au NCs) onto quaternary I-III-VI copper indium sulfide selenide nanoparticles (CuInSSe NPs) and compare them with results obtained with pure copper indium disulfide nanoparticles ($CuInS_2$ NPs). The growth behaviour of gold nanocrystals as well as the structure and the optical properties of resulting nanostructures were studied by transmission electron microscopy (TEM), energy dispersive X-ray analysis (EDX), X-ray diffraction (XRD), and UV-Vis-absorption spectroscopy.

2. Experimental

2.1. Materials

Copper (I) chloride (CuCl), indium chloride ($InCl_3$, 98%), 1-dodecanethiol (DDT, 98%), tri-*n*-octylphosphine (TOP, 90%), gold (III) chloride ($AuCl_3$, 99%), didodecyldimethylammonium bromide (DDAB, 90%) were purchased from Aldrich; selenium powder (Se, 99.99%) from ChemPur; 1-octadecene (ODE) from Merck; dodecylamine (DDA, 98%) from Acros Organics. All chemicals were used without further purification.

2.2. Synthesis of CuInSSe Nanoparticles

The CuInSSe nanoparticles were synthesized using a modification of a previously reported method [27]. In brief, CuCl (0.1 mmol) and $InCl_3$ (0.1 mmol) were mixed with DDT (1 ml) and ODE (2 ml) at room temperature. Afterwards, the solution was heated to 180 °C, a selenium solution in TOP (0.2 mmol selenium dissolved in 0.2 ml TOP) was injected into the reaction mixture, and then the reaction temperature was kept at 180 °C for an hour. After the reaction mixture was cooled to room temperature, 10 ml acetone was added to precipitate the nanocrystalline product. The precipitated nanocrystals were washed with $CHCl_3/CH_3OH$ (1 : 3, v/v) three times and then dissolved in toluene to get the nanocrystal solution.

2.3. Synthesis of Hybrid Nanostructures

The procedure of growth of Au NCs is similar to a previously reported procedure for CdSe NCs [17]. Briefly, a gold precursor solution was prepared by dissolving $AuCl_3$ (12.5 mg), DDA (73 mg), and DDAB (41.7 mg) in toluene (3.125 ml) by sonication. This gold growth solution was added dropwise to a solution of CuInSSe NPs in toluene at room temperature while vigorously stirring. The reaction was stopped by precipitating the hybrid nanocrystals with methanol. The nanocrystals were redissolved in toluene for characterization.

The synthesis of $CuInS_2$-based nanostructures was conducted in the same way.

2.4. Characterization

The TEM images were taken on a Zeiss EM 902A transmission electron microscope with an acceleration voltage of 80 kV. The samples for TEM measurement were prepared by depositing a drop of a diluted toluene solution of nanoparticles on a carbon-coated copper grid and dried at room temperature.

X-ray diffraction (XRD) was measured with a PANalytical X'Pert PRO MPD diffractometer operating with Cu K_α radiation, Bragg–Brentano $\theta - 2\theta$ geometry, and a goniometer radius of 240 mm. Samples for XRD measurement were prepared by drying the purified product on the silicon sample holders. Rietveld refinement of the diffraction patterns was conducted using the program MAUD [28]. The patterns were fitted using a polynomial background and default instrument line broadening from the MAUD software. The anisotropic size-strain model developed by Popa [29] was used to account for anisotropic crystallite shapes, while texture effects were included by the harmonic texture model [30].

The integral stoichiometry was obtained by the EDAX detector integrated into a FEI Quanta 200 3D scanning electron microscope.

Absorption spectra were recorded in hexane on a Carry 100 absorption spectrophotometer (Varian), using 1 cm path length quartz cells.

3. Results

3.1. Semiconductor CuInSSe Nanoparticles

The original semiconductor CuInSSe nanoparticles are shown in Figure 1. They have trigonal pyramidal

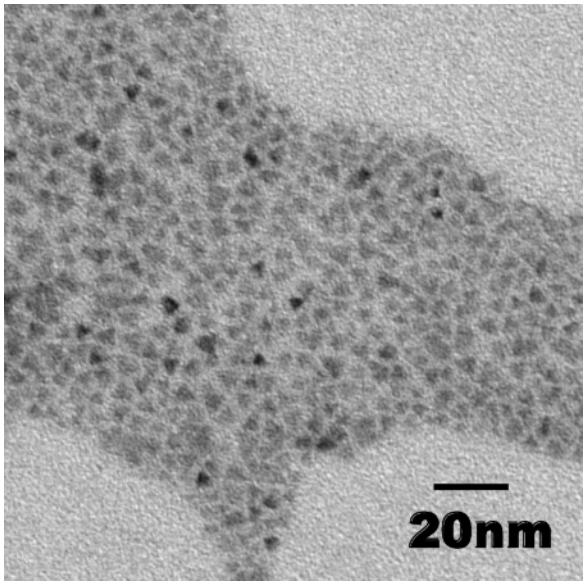

Fig. 1. TEM image of the CuInSSe NPs.

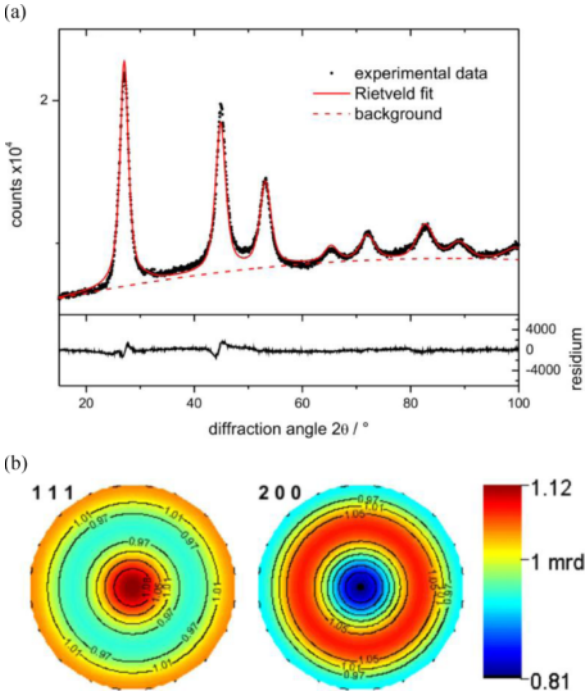

Fig. 2 (colour online). (a) Powder X-ray diffraction patterns of the CuInSSe NPs. The experimental data (dots) are plotted together with a Rietveld fit (red line). (b) Reconstructed pole figures resulting from refinement according to the applied texture model. The (111) planes have a high probability to be oriented parallel to the sample holder.

shape and an average size of 5.5 ± 0.8 nm. The synthesis route was similar to the one for $CuInSe_2$ NPs developed by Zhong et al. [27], where CuCl and $InCl_3$ were used as copper and indium precursors, DDT as the ligand, and ODE as the non-coordinating solvent. Changing the concentration of DDT as well as the molar ratio of copper (or indium) to selenium precursors leads to formation of CuInSSe NPs. Keeping the other conditions the same, the average size almost did not change; the $CuInSe_2$ NPs from [27] had an average size of 6 nm. But the element ratio was changed. According to energy dispersive X-ray (EDX) analysis, the ratio Cu : In : S : Se was found to be 0.86 : 1 : 0.65 : 1.35, while Zhong's nanoparticle composition was $Cu_1In_{1.1}Se_{1.6}$ according to inductively coupled plasma atomic emission spectroscopy (ICP-AES) [27]. Thus, in our reaction the thiols partly decompose and serve as a sulfur source for the reaction.

The structure and the composition of CuInSSe NPs were further investigated with powder X-ray diffraction. At room temperature, bulk I-III-VI semiconductors crystallize in the chalcopyrite structure, which is a superstructure of the zinc blende type with an a/c ratio of 2 [31]. At higher temperatures, the cations disorder in the cation sublattice, and the chalcopyrite structure reverts to a zinc blende structure. In contrast to the bulk materials, nanocrystalline I-III-VI semiconductors form stable cation disordered polymorphs with zinc blende or wurtzite structure also at room temperature [31 – 34]. The Rietveld analysis of the XRD pattern of our CuInSSe NPs revealed that they crystallize in the zinc blende structure (Fig. 2). The lattice parameter was refined to 5.72 Å. This value lies between the lattice parameters for $CuInS_2$ and $CuInSe_2$ (5.52 Å and 5.78 Å, respectively). Assuming a linear dependence of the lattice parameters on the composition, we determined the fraction of the sulfur atoms incorporated into the lattice of the CuInSSe particles to be 0.27. Such a value is smaller than the one obtained from EDX measurements (0.48), which gives an indication for a sulfur rich surface. The latter is a reasonable assumption, because of the presence of thiols (DDT) in the reaction solution which bind to the CuInSSe surface and form the ligand shell.

As is obvious from the TEM images, the particles do not have a preferential growth direction. Thus, we used an isotropic model for determining the sizes of the crystallites. The value of 6.3 nm is in good agree-

ment with the size obtained from TEM. Figure 2 shows a reconstructed pole figure deduced from the texture analysis of the sample. In the TEM images, the particles which have a tetrahedral shape lay on one of the (111) surfaces terminating the tetrahedron. This indicates that texture effects might be found in the XRD patterns. Indeed, the poles of the (111) lattice planes are found primarily in the center of the projection plane, indicating that the (111) planes are preferentially oriented parallel to the sample holder.

The absorption spectrum is shown in Figure 3. Compared to the values for the bulk materials (1.04 eV for $CuInSe_2$ [35] and 1.53 eV for $CuInS_2$ [36]) the band gap of our CuInSSe NPs is blue-shifted due to the quantum confinement effect.

3.2. Hybrid Nanostructures

The resulting hybrid nanostructures are shown in Figure 4. Comparison with the original CuInSSe NPs shows that the size and the shape of the nanocrystals did not significantly change after the reaction with gold, the size of the semiconductor part is 4.2 ± 0.8 nm. However, after the reaction between CuInSSe and gold precursor solution particles with a higher contrast can be found on the vertexes of pyramidal CuInSSe NPs. The size of these particles was estimated to be 2.3 ± 0.4 nm. Apparently, Au NPs selectively grow onto vertexes of CuInSSe pyramides, which have a high surface energy and might be less efficiently protected by organic ligands. These two reasons facilitate selective growth of metal NCs onto semiconductor NPs [14, 17].

We studied the structure of this hybrid material with X-ray diffraction. Figure 5 shows the diffraction pattern obtained, together with the results of the Rietveld analysis. All the reflections are significantly broadened indicating the nanocrystalline nature of the sample. The presence of some amount of an amorphous material also cannot be excluded. As expected, gold nanocrystals can be found in the hybrid material. Their size was calculated to be 4 nm, using an isotropic shape model. This value is larger than the size obtained from TEM images. The other phase that could be identified from the XRD measurement consists of small nanoparticles (1.5 nm) of elemental selenium. We found some texture effects for the selenium phase, using a harmonic texture model [30]. Interestingly, a comparison of the reconstructed pole figures shows some similarities for the (100) and (011) planes in selenium (3.24 Å and 2.74 Å, respectively) and (111) and (200) planes in the original CuInSSe particles (3.30 Å and 2.86 Å, respectively). Even though, we cannot find a crystalline CuInSSe phase in the diffraction pattern after the reaction with gold, selenium particles seem to have a preferred orientation, which is related to the preferred orientation of the CuInSSe tetrahedra used for this reaction. Thus, the reaction with gold converts some part

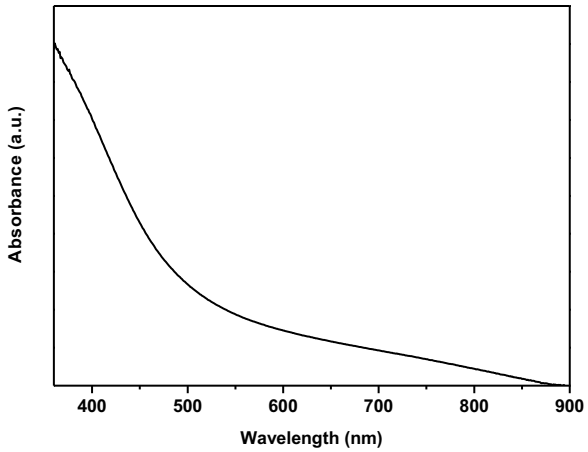

Fig. 3. Absorption spectrum of the original CuInSSe NPs.

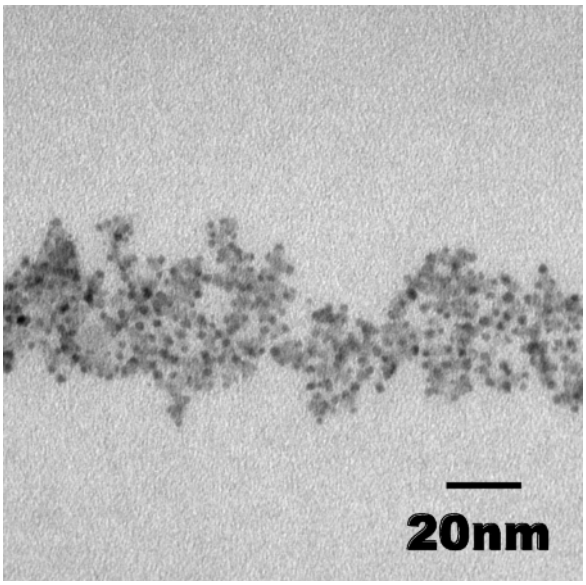

Fig. 4. TEM image of the CuInSSe-based hybrid nanostructures.

of the CuInSSe nanoparticles to elemental selenium. This particle probably remains attached to the remaining CuInSSe part. However, we cannot distinguish between CuInSSe and selenium in the TEM imgages, because both materials have similar contrast.

The UV-Vis-absorption spectrum of hybrid nanocrystals is shown in Figure 6. The plasmon resonance of Au NPs [17] has not been observed, because of the relatively small size of metallic nanocrystals [1]. The absorption offset of the hybrid nanostructure is blue-shifted compared with the original CuInSSe NPs. One reason for the blue shift can be the reduced size of the semiconductor part of the hybrid material, compared with the original CuInSSe tetrahedra. We can, however, not exclude also changes in the composition of the CuInSSe nanocrystals.

We characterized the samples by EDX analysis, in order to determine the composition of the nanocrystals after the reaction with gold. Compared with the original CuInSSe NPs, the resulting hybrid nanostructures have a different ratio between copper, indium, sulfur, and selenium, furthermore, gold could be detected. We found a ratio of 1 : 1 : 1 : 5 : 14 for Cu : In : S : Se : Au. The element ratio in the semiconductor part can change after the reaction with the gold precursor [37] because the semiconductor material plays the role of the reducing agent for gold ions. This mechanism of the reaction proposed by Khalavka and Sönnichsen [37] for CdTe/Au nanostructures seems to hold also for our materials:

$$3\mathrm{Se}^{2-} + 2\mathrm{Au}^{3+} \rightarrow 2\mathrm{Au}^{0} + 3\mathrm{Se}\,.$$

Gold reduction takes place on the surface of CuInSSe NPs. The change of the elemental ratio In : S : Se from 1 : 0.65 : 1.35 in initial CuInSSe NPs to 1 : 1 : 5 in the hybrid nanostructures is surprising at first, when taking into account the difference between the values of the reduction potentials of selenium and sulfur (Se^{2-}: -0.92 V, S^{2-}: -0.48 V) [37]. Selenium oxidizes much faster than sulfur and should be used up more easily during the reaction. If selenium goes into solution after this reaction, sulfur rich particles should be obtained. Indeed, the ratio between indium and sulfur changes from 1 : 0.65 in the original sample to 1 : 1 in the hybrid material. Taking into account the results of the XRD measurements (Fig. 5) showing that elemental selenium is present in the samples, also the increase of the selenium content can be explained. Selenium remains partly in the sample, while some of the cations go into the solution. These changes of the composition of the sample are accompanied by changes in the crystallinity of the CuInSSe material.

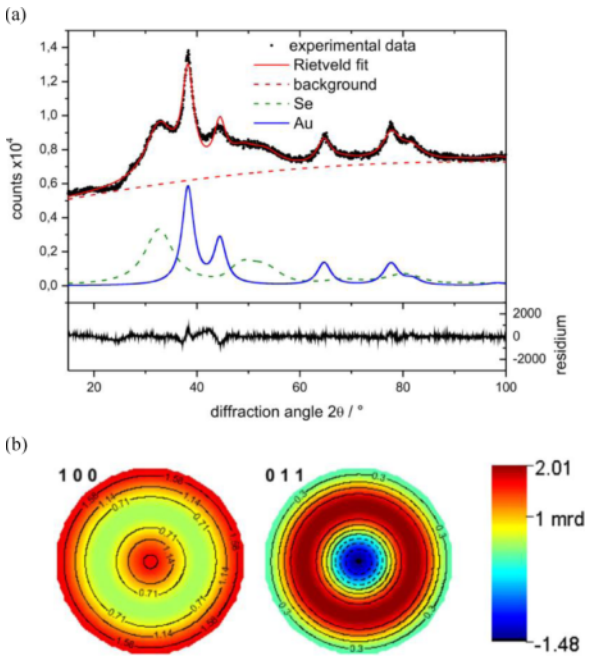

Fig. 5 (colour online). (a) Powder X-ray diffraction patterns of the hybrid nanostructures. The experimental data (dots) are plotted together with a Rietveld fit (red line) and the deconvolution into two phases, selenium (green line) and gold (blue line). (b) Reconstructed pole figures resulting from refinement according to the applied texture model. The (100) planes of selenium have a high probability to be oriented parallel to the sample holder.

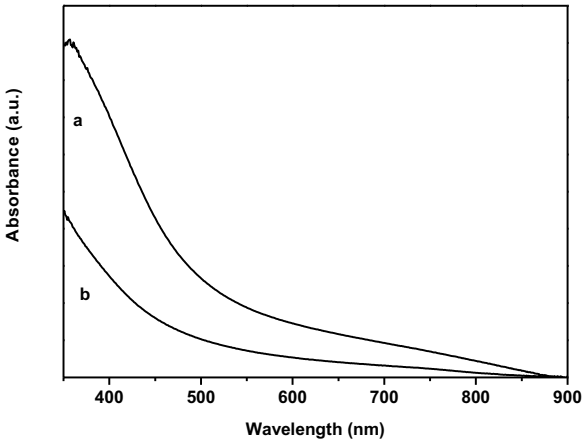

Fig. 6. Comparison of the absorbtion of the original CuInSSe NPs (a) and resulting hybrid nanostructures (b).

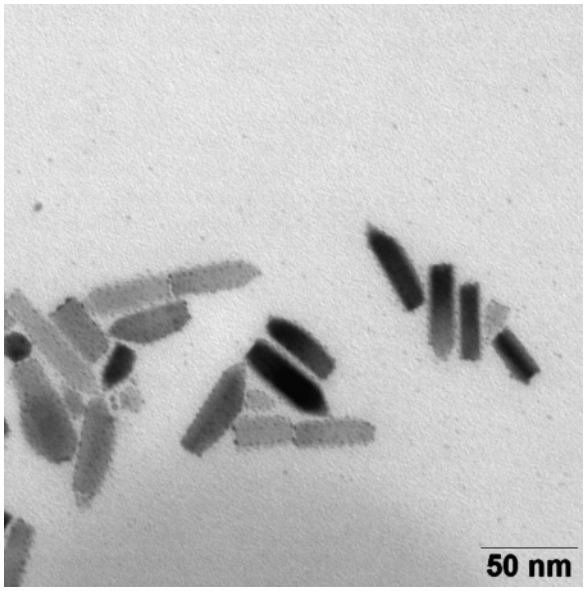

Fig. 7. TEM image of the $CuInS_2$/Au NPs.

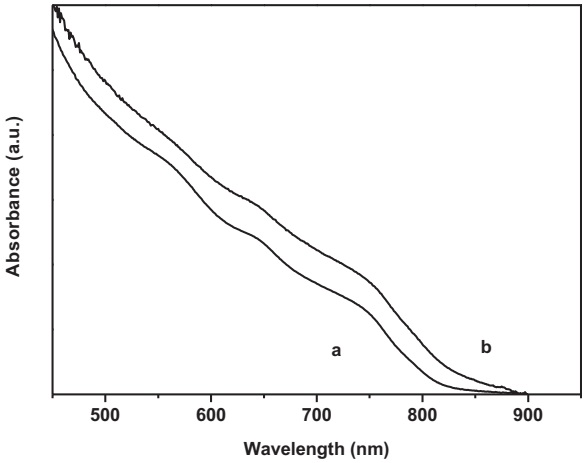

Fig. 8. Comparison of the absorbtion of the original $CuInS_2$ NPs (a) and $CuInS_2$/Au hybrid nanostructures (b).

It has been shown by the Banin group [1] that the heterogeneous growth behaviour of gold nanocrystals on nanorods is significantly different for different cadmium chalcogenides, such as CdSe and CdS [1]. We applied $CuInS_2$ NPs, synthesized according to a method described previously [23], in order to find out, whether a selective growth of gold nanocrystals is also possible on other I-III-VI NPs. In this reaction, the growth behaviour of gold is different. The reduction of gold takes also place on the surface of the $CuInS_2$ NPs, but the selective growth was not observed. Although the $CuInS_2$ NPs chosen for this reaction possess regions of high surface curvature, relatively small gold particles appear at random places on the whole surface of the semiconductor (Fig. 7). According to other studies [1], defects also provide high energy sites for nucleation and growth of Au NCs. Also in our study, the presence of defects on the surface of $CuInS_2$ NPs is relatively likely, as can be seen from their low emission quantum efficiency (results not shown here). Thus, we conclude that growth of Au NCs on the surface of $CuInS_2$ NPs preferentially takes place on the surface defects.

The absorption spectra of the original $CuInS_2$ NPs and the $CuInS_2$/Au hybrid nanoparticles are shown in Figure 8. The absorption offset of hybrid NPs is red-shifted. As has been shown for other materials, the red shift originates from delocalization of the electrons over the whole semiconductor–metal nanohybrid material, and might be also due to the increase of the dielectric constant of the shell around the semiconductor in the presence of metal particles [12, 17]. We do not observe any changes in the shape and in the size of the $CuInS_2$ NPs, thus, the redshift of the absorption offset indicates the formation of metal–semiconductor hybrid nanostructures in solution, and not later, e. g., under the beam in the transmission electron microscope.

4. Conclusions

In summary, CuInSSe/Se/Au nanostructures have been produced by the growth of Au NCs onto the previously prepared CuInSSe NPs. The mechanism of this reaction is based on a reduction of a gold precursor on the vertexes of the CuInSSe pyramides, according to the results of the TEM and EDX analysis. The reaction leading to the formation of gold nanocrystals has a strong influence onto the structure of the semiconductor part of the hybrid material, because CuInSSe plays the role of the reducing agent for gold ions. Thus, heterostructure nanocrystals grow through the reaction of a sacrificial component of the semiconductor part. During this reaction, elemental selenium particles are formed, and the size and the crystallinity of the CuInSSe part of the hybrid nanostructure are reduced. However, the EDX measurements reveal that the particles still contain copper and indium, and, in spite of their lower crystallinity, absorption of the CuInSSe nanoparticles still can be observed. In contrast to these

results, experiments with particles which do not contain selenium ($CuInS_2$ NPs), did not show any selectivity of the Au NCs growth, but also no changes in the size and shape of the semiconductor part of the hybrid structure were observed. Our results show that semiconductor–metal hybrid nanostructures can be obtained from I-III-VI semiconductor nanocrystals, and gold particles preferentially grow on surface sites having high energy (defects, or places with high curvature). A comparison between the reactions of CuInSSe and $CuInS_2$ NPs shows that the presence of selenium facilitates the growth of Au NCs and enhances the selectivity of the reaction.

Acknowledgements

We thank Erhard Rhiel and Heike Oetting for assistance in obtaining TEM images. We thank Marta Kruszynska for synthesizing $CuInS_2$ nanoparticles. E. W. gratefully acknowledges personal funding within the 'EWE-Nachwuchsgruppe Dünnschicht-Photovoltaik' by the EWE AG, Oldenburg.

[1] A. E. Saunders, I. Popov, and U. Banin, J. Phys. Chem. B **110**, 25421 (2006).
[2] R. Costi, A. E. Saunders, and U. Banin, Angew. Chem. Int. Ed. **49**, 4878 (2010).
[3] C. D. M. Donegá, Chem. Soc. Rev. **40**, 1512 (2011).
[4] L. Carbone and P. D. Cozzoli, Nano Today **5**, 449 (2010).
[5] K. M. AbouZeid, M. B. Mohamed, and M. Samy El-Shall, Small **7**, 3299 (2011).
[6] J. I. Climente, J. L. Movilla, G. Goldoni, and J. Planelles, J. Phys. Chem. C **115**, 15868 (2011).
[7] P. V. Kamat, J. Phys. Chem. C **112**, 18737 (2008).
[8] S. Huang, J. Huang, J. Yang, J. J. Peng, Q. Zhang, F. Peng, H. Wang, and H. Yu, Chem. Eur. J. **16**, 5920 (2010).
[9] J. Gao, H. Gu, and B. Xu, Acc. Chem. Res. **42**, 1097 (2009).
[10] R. Hao, R. Xing, Z. Xu, Y. Hou, S. Gao, and S. Sun, Adv. Mater. **22**, 2729 (2010).
[11] Y. Kobayashi, Y. Nonoguchi, L. Wang, T. Kawai, and N. Tamai, J. Phys. Chem. Lett. **3**, 1111 (2012).
[12] N. M. Dimitrijević, T. Rajh, S. P. Ahrenkiel, J. M. Nedeljković, O. Mićić, and A. J. Nozik, J. Phys. Chem. B **109**, 18243 (2005).
[13] B. Gao, Y. Lin, S. Wei, J. Zeng, Y. Lia, L. Chen, D. Goldfeld, X. Wang, Y. Luo, Z. Dong, and J. Hou, Nano Res. **5**, 88 (2012).
[14] J. Yang, H. I. Elim, Q. Zhang, J. Y. Lee, and W. Ji, J. Am. Chem. Soc. **128**, 11921 (2006).
[15] M. Berr, A. Vaneski, A. S. Susha, J. Rodríguez-Fernández, M. Döblinger, F. Jäckel, A. L. Rogach, and J. Feldmann, Appl. Phys. Lett. **97**, 93108 (2010).
[16] G. Menagen, J. E. Macdonald, Y. Shemesh, I. Popov, and U. Banin, J. Am. Chem. Soc. **131**, 17406 (2009).
[17] T. Mokari, E. Rothenberg, I. Popov, R. Costi, and U. Banin, Science **304**, 1787 (2004).
[18] L. Carbone, A. Jakab, Y. Khalavka, and C. Sönnichsen, Nano Lett. **9**, 3710 (2009).
[19] J. Yang, L. Levina, E. H. Sargent, and S. O. Kelley, J. Mater. Chem. **16**, 4025 (2006).
[20] W. Shi, H. Zeng, Y. Sahoo, T. Y. Ohulchanskyy, Y. Ding, Z. L. Wang, M. Swihart, and P. N. Prasad, Nano Lett. **6**, 875 (2006).
[21] R. Xie, M. Rutherford, and X. Peng, J. Am. Chem. Soc. **131**, 5691 (2009).
[22] P. M. Allen and M. G. Bawendi, J. Am. Chem. Soc. **130**, 9240 (2008).
[23] M. Kruszynska, H. Borchert, J. Parisi, and J. Kolny-Olesiak, J. Am. Chem. Soc. **132**, 15976 (2010).
[24] M. Kruszynska, H. Borchert, J. Parisi, and J. Kolny-Olesiak, J. Nanopart. Res. **13**, 5815 (2011).
[25] Y. M. Xu and Q. Li, Nanoscale **3**, 3238 (2011).
[26] Q. Zhang, J. J. Wang, Z. Jiang, Y. G. Guo, L. G. Wan, Z. Xiea, and L. Zheng, J. Mater. Chem. **22**, 1765 (2012).
[27] H. Zhong, Y. Li, Y. Mingfu, Z. Zhu, Y. Zhou, C. Yang, and Y. Li, Nanotechnology **18**, 025602 (2007).
[28] L. Lutterotti, D. Chateigner, S. Ferrari, and J. Ricote, Thin Solid Films **450**, 34 (2004).
[29] N. C. Popa, J. Appl. Cryst. **31**, 176 (1998).
[30] N. C. Popa, J. Appl. Cryst. **25**, 611 (1992).
[31] Y. Qi, Q. Liu, K. Tang, Z. Liang, Z. Ren, and X. Liu, J. Phys. Chem. C **113**, 3939 (2009).
[32] M. E. Norako and R. L. Brutchey, Chem. Mater. **22**, 1613 (2010).
[33] S. K. Batabyal, L. Tian, N. Venkatram, W. Ji, and J. J. Vittal, J. Phys. Chem. C **113**, 15037 (2009).
[34] J. J. Wang, Y. Q. Wang, F. F. Cao, Y. G. Guo, and L. J. Wan, J. Am. Chem. Soc. **132**, 12218 (2010).
[35] M. A. Malik, P. O'Brien, and N. Revaprasadu, Adv. Mater. **11**, 1441 (1999).
[36] B. Koo, R. N. Patel, and B. A. Korgel, Chem. Mater. **21**, 1962 (2009).
[37] Y. Khalavka and C. Sönnichsen, Adv. Mater. **20**, 588 (2008).